PROPERTIES OF DIELECTRIC IMAGE LINES

D. D. King
Radiation Laboratory
The Johns Hopkins University
Baltimore, Maryland

Summary

The properties of a dielectric rod on an image surface are reviewed, and experimental results on straight sections, various bends, and a twist are presented. Techniques for measuring insertion parameters and field distributions are described.

Introduction

Dielectric guides for millimeter waves are generally simpler to fabricate than hollow tubes, but more difficult to use in transmission and circuit applications. Problems of supports, bends and shielding are not easily solved for low-loss dielectric guides. The lower the loss, the worse these problems become. This is a consequence of the fact that the dipole mode, which gives lowest loss, must be loosely bound to the dielectric to achieve minimum attenuation. Indeed, at the cost of occupying an arbitrarily large cross-section about the dielectric, the attenuation per unit length can be reduced to as low a value as desired. The effective cross section occupied by the wave is measured in square wavelengths. Therefore, significant cross-sectional areas and attendant large reductions in attenuation are only feasible in the millimeter region.

Since the dipole mode exhibits a plane of symmetry containing the axis of the rod, an image plane may be used to replace half of the rod and surrounding space. Such an image system reduces the required cross-section by one-half, and also largely eliminates the support and shielding problems.

The feasibility of the dielectric image waveguide has been demonstrated,[1] but the full possibilities of this scheme remain to be explored. Additional results on the properties of various cross-sections, and of bends and twists are described in this paper.

Dielectric Image Guide

The theory of straight dielectric rods with circular cross-sections has been developed by Elsasser.[2] His results show that the phase constant of the dipole mode is very nearly that of free space for operation in the region beyond the cut-off of TM and TE modes. This is consistent with the fact that most of the power is carried outside the dielectric. The attenuation is given by

$$A = 2729\ (\varepsilon_d \phi/\lambda_o) R \ (\text{db/m}) \qquad (1)$$

Where $\phi = \sigma/\omega\varepsilon_d\ \varepsilon_o$ (power factor of dielectric)

ε_d = relative dielectric constant

λ_o, ε_o = free space wavelength in cm

dielectric constant

The factor R is a complicated function of the diameter and ε_d. The resulting attenuation for $\varepsilon_d = 2.56$, $\phi = .001$ is plotted in Fig. 1. This calculation of attenuation relies on an accurate knowledge of the power factor of the dielectric material, which limits the accuracy attainable. (In this connection, Eq. (1) and the measured value of attenuation might prove useful in determining the power factor of dielectrics in the millimeter region.)

The attenuation of an image system with perfectly conducting image plane is also given by Eq. (1). A calculation of the contribution of finite conductivity to the attenuation can be made from the loss-less field distribution on the image surface. This has not yet been undertaken. Probable errors in the value of dielectric power factor tend to obscure the correction so obtained.

The phase and attenuation constants of circular dielectric rods have been measured and are in agreement with theory.[3] Measurements on image rods of semi-circular cross-section also confirm the theory.

A straight section with launching horn and section for inserting the dielectric is shown in Fig. 2. The optimum horns are designed for image plane use, and are therefore not symmetrical. The actual aperture is 5 x 2" and length is 14". To excite the dipole mode fully, the dielectric must be extended beyond the horn into the waveguide. The insertion sections for this permit easy adjustment of the dielectric strip through choke tubes. The dielectric consists of a split RG59/U cable insulator whose original diameter was .134". The image surface is a 6"

strip of .018" soft copper on a plywood base. Some ripples remained in the metal, and the dielectric was not everywhere in contact with the image surface. The table below shows the measured input reflection coefficient and transmission loss for several configurations.

TABLE I

Configuration	Insertion Loss	Input VSWR
Dielectric insertion sections and horn launchers butted together	1.6 db	1.7
As above, 1 meter spacing between launchers	2.4 db	1.1

The effect of changes in the dielectric cross-section plated on the image surface, and of bends and twists in this surface are difficult to calculate. However, measurements on these modifications have been made which are in agreement with qualitative interpretations of the wave propagation involved. Results are presented next on various bends, a twist, and several straight sections with different dielectric cross-sections. A loosely coupled wave is used throughout. This avoids TM and TE modes, and assures a low value of attenuation. The overall lengths used are also kept short, since the principal application of the image system appears to be in circuit elements and short transmission sections, rather than in long cross-country lines.

Bends in Image Guide

Bends in conventional guides are classified in E-plane or H-plane. In an image system, the identification of these two planes is particularly easy. However, in addition to the H-plane bend, two E-plane bends exist, one convex, the other concave. Typical adjustable bends of each type are shown in Figs. 3,4,5. For the plane and concave bends, the dielectric was cemented with amphenol cement. This cement produces no noticeable effect if used sparingly. Since the wave is loosely bound to the rod, curvature of the rod should permit a portion of the energy in the space around the rod to proceed straight on without following the bend dielectric. In the limiting case of an indefinitely thin rod, the resulting plane wave certainly proceeds in this fashion. An approximate theory has been developed for slight curvatures which confirms this reasoning:[4] on the outer or convex side of the bend radiation takes place, while on the inner or concave side only evanescent waves develop.

By symmetry, the H-plane bend should exhibit identical properties in both circular rod and image rod systems. This should also be approximately true for the convex E-plane bend since here the path of radiation is away from the image surface. On the other hand, the concave E-plane bend cannot radiate in the same fashion since the curved image surface deflects all waves proceeding along the projection of the straight section. Therefore, one may conclude that the concave E-plane bend should resemble more closely the performance of the other two bends equipped with reflectors.

Experimental data on the three bends with phosphor bronze image surfaces is shown in Fig. 6. Here the insertion loss of the bend is plotted for three different radii of curvature. Two interesting trends appear:

1) the concave bend has the lowest insertion loss, and improves with increasing radius of curvature,

2) the convex and plane bends are very lossy for the radii of curvature tested but improve markedly with a reflector when the radius of curvature is small.

The optimum location of the reflector is always precisely at a 45° angle and at the intersection of the two guide axes; i.e., as predicted by geometrical optics. Since the end points of the bends were kept fixed, the larger radii of curvature actually shorten the total length of guide, between the transitions. However, this effect is negligible because of the low loss of the straight guide. The input VSWR with output matched showed no significant trends and remained between 1.20 and 1.28 for all the bends tested. This indicates that radiation and not reflection produces the insertion loss.

The performance of a 90° twist accomplished in a length of 40 cm. was less satisfactory, giving an insertion loss of about 7 db. Because of the difficulty in fabricating twists, no other lengths were tested. The twist tested is shown in Fig. 7.

Effect of Cross-Section

Two cross-sectional areas are needed to describe a wave loosely coupled to a dielectric rod; they are, 1) the cross-section of the dielectric, and 2) the effective total cross-section of the wave, as defined by the terminals used. The theory of Elsasser permits exact calculation only for a circular dielectric cross-

section and an infinite outer boundary. For other shapes of the dielectric and for a finite effective cross-section, a qualitative description of loosely coupled waves is more useful.

Two observations are helpful in this connection. First, the small dielectric cross-sections used in the dipole mode do not permit any transverse resonances within the dielectric, and second, the concentration of the field about the rod depends upon the volume of dielectric in regions of high electric field. The properties of the transmission system should therefore be insensitive to the exact shape of the dielectric cross-section, but strongly dependent upon the total cross-sectional area occupied by the dielectric.

Measured distributions of the field in the effective cross-section are shown in Fig. 8. These curves bear out the fact that the shape of the dielectric is not critical, provided an adequate dielectric volume is located in regions of high electric-field. The more tightly bound waves appear at the top of the graph, the loosely bound waves at the bottom.

Losses in straight dislectric lines are two-fold: (1) dielectric loss, and, (2) radiation loss. This neglects conduction loss on image surface for image lines. The dielectric loss is evidently proportional to the concentration of the field in the dielectric and hence increases with dielectric cross-section. Radiation loss is proportional to the power carried outside the effective cross-section and becomes negligible for large effective cross-sections. Both dielectric and radiation loss contribute to the attenuation per unit length of line. However, by varying the effective cross-section, the two can be separated. Measured losses for various dielectric and effective cross-sectional areas are shown in Table II. Also included in the table is the measured

TABLE II

Dielectric cross-section	Effective cross-sectional radius	Line-Loss in db/100 ft.	Termination loss γ in db per termination
Inverted half-round radius .066"	6"	.9	.15
	3"	1.6	.12
.084" square	6"	.3	.28
	3"	1.5	.16
Half-round radius .066"	6"	.5	.17
	3"	1.5	.13

loss in the terminations of the resonant length of line. These terminations were flat semi-circular sheets of dural.

The data presented is rather limited because of measuring difficulties. However, the following trends are noticeable:

1) For the 6" effective radius, line loss is small and depends upon the dielectric cross-section; for the 3" radius, line loss is greater and independent of dielectric cross-section.

2) For the 6" effective radius, the termination loss is consistently greater than for the 3" radius. Termination loss is greatest when line loss is smallest.

For large end plates, the power transfer is confined largely to the effective cross-section, hence the wave does not diverge rapidly from the launchers. The radiation loss is then confined to a constant reflection loss which becomes larger as the wave is decoupled.

For small end plates, the wave diverges from the launchers. Therefore, the magnitude of the reflection loss at the end faces of the resonator depends upon their spacing. Consequently, a large radiation loss appears in α as an increasing loss with length. The constant termination loss γ is correspondingly smaller.

The fact that the radiation loss may appear as a contribution to the line loss rather than to the termination loss is contrary to the description of the wire wave given by Goubau[5] for long wire lines. For short lengths, it is clear that the radiation loss increases with line length, since the wave is diverging from the launching area to the unbounded cross-section demanded by the mode of propagation. The larger the launcher, the slower rate of divergence will be. Essentially, the launching device whether a horn or a reflecting plate may be looked upon as a highly directive antenna whose virtual source is far behind it. For large spacings of this virtual source, the spreading of the wave per unit length becomes negligible. Radiation loss then can properly be lumped with the terminations. The fact that the radiation loss is a function of plate separation has been proved rigorously by Roberts for a similar resonator consisting of flat end plates and a single wire line.[6]

Measurement Techniques

The apparatus for measuring insertion loss and input reflection coefficient is shown in Fig. 9. The insertion loss was measured by substitution of a calibrated attenuator. Input reflections were obtained from a carefully balanced magic tee. By placing a matched load at the

output end of the test section, the input reflection coefficient could be read directly. The maximum and minimum values of input reflection obtained with a sliding short at the output end yielded an additional value of the insertion loss.

The reflection method of measuring insertion loss gave good results for low insertion loss. For high attenuation, the sliding plunger in the output of the test section produced too small a change at the unput for accurate results.

The system described above using a matched hybrid was checked with sliding shorts in both arms, as shown in Fig. 9. The resulting circular locus obtained in the Smith chart permits calculation of the insertion loss and input reflections by the Deschamps procedure. This procedure was used for determining the insertion loss of straight sections and of the launchers, where relatively low total attenuation was involved.

Attenuation for straight lengths of line was obtained from the Q of resonant lengths. The resonator is shown in Fig. 10. Tilt and position of the end plates could be adjusted by hand to maximize the resonant response at the desired position on the display. A 1/2" slab of brass with smooth but unpolished surface served as the image surface. The semi-circular dural end plates have 1/4" diameter coupling apertures, and are fitted with an L-shaped choke groove at the base to avoid contact troubles.

The system for measurements on the resonator is shown in Fig. 11. With square-wave modulation the insertion loss was measured on meters 1 and 2. With sawtooth modulation, the loaded Q was measured as follows: A precision attenuator in the output line was first set at 3 db and the resonance curve positioned as in Fig. 12. Next, the attenuator was set to zero and the base lines realigned. The marker gaps could then be set on the intersections at the 3 db points. Twice the receiver dial reading then furnished the half-power width Δf. Since the total frequency excursion is about 30 Mc., only relatively high-Q resonators could be tested in this fashion.

Line loss and termination loss may be determined from the slope and intercept of a plot of $1/Q_x$ length vs. length.[7] A typical plot of this type is shown in Fig. 13. The contribution of coupling losses is indicated by the dotted curves plotted from the relation

$$Q_u = \left(\frac{1}{1-T^{\frac{1}{2}}}\right) Q_L$$

Where T = insertion loss

The measurements of field distribution were made by inserting an 8 cm. length of IRC card 1/8" wide parallel to the axis of the line. The curves shown represent the resulting change in transmission through the resonator. For insertion loss greater than 20 db, the transmission is closely proportional to Q_u^2, which in turn is inversely proportional to the square of the power dissipated. If most of the dissipation is in the resistance card, a plot of attenuation due to the card is also a plot of $(E^2)^2$. By halving the decibel scale, a plot of E in decibels is obtained.

An alternative procedure relies on an unipol about a half-wavelength long mounted on a flat metal shim. This scatterer dissipates energy and hence provides similar data. However, the high VSWR requires careful axial positioning, and location under the dielectric is not possible. A photograph of both dissipative devices is shown in Fig. 14.

Conclusions

Dielectric image lines are uncritical in the exact shape or position of the dielectric, and show promise of convenient application in bends and straight sections in the millimeter region. Advantages such as ease of manufacture by extrusion on a metal sheet, and iris coupling from below remain to be evaluated. However, from the preliminary date at hand, it appears that dielectric image circuits at millimeter waves have lower loss in straight sections and are easier to fabricate than corresponding waveguide elements. Loss in bends may be reduced by a concave or reflector design. Increasing the dielectric cross-section slightly in the bend also appears desirable to confine the field more closely. The necessary cross-sectional area is perhaps the principal objection to the image line, and this diminishes rapidly with decreasing wavelength.

References

1. King, D.D., Jour. of Appl. Phys., 23, p. 669; June, 1952.
2. Elsasser, Jour. of Appl. Phys., 20, p. 1193; December, 1949.
3. Chandler, Jour. of Appl. Phys., 20, p. 1188; December, 1949.
4. Barlow, Jour. IEE-III 100;November,1953.
5. Goubau, Jour. of Appl. Phys. 21, p. 1119; 1950.
6. Roberts, T.E., Jr., Jour. of Appl. Phys., 24, p. 63; 1953.
7. Scheibe, King, B.G., and Van Zeeland, Jour. of Appl. Phys. 25, p. 795; 1954.

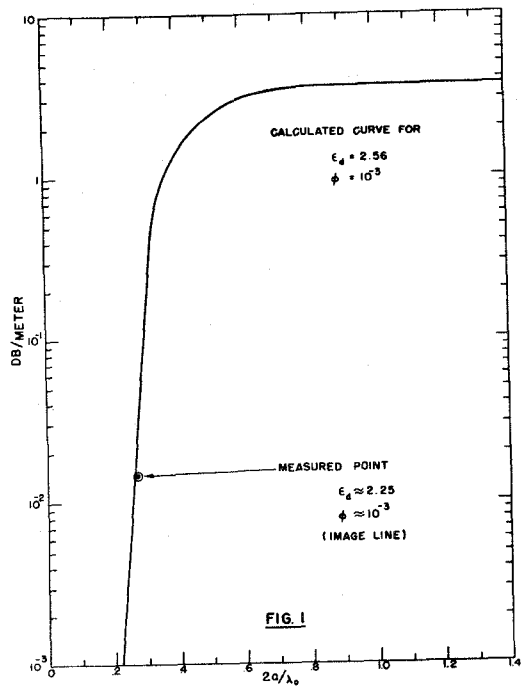

Fig. 1 - Theoretical attenuation of dipole mode.

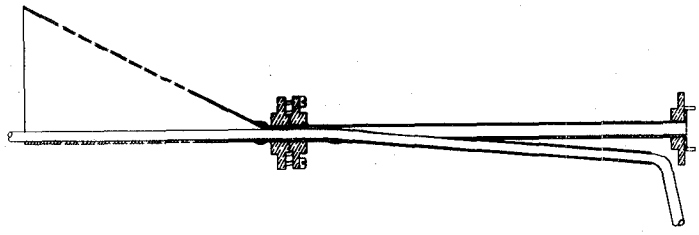

Fig. 2 - Image horn launchers and dielectric insertion sections.

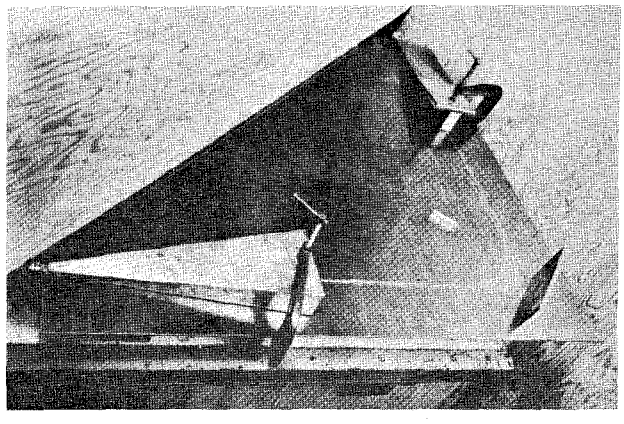

Fig. 3 - H-plane bend with reflector.

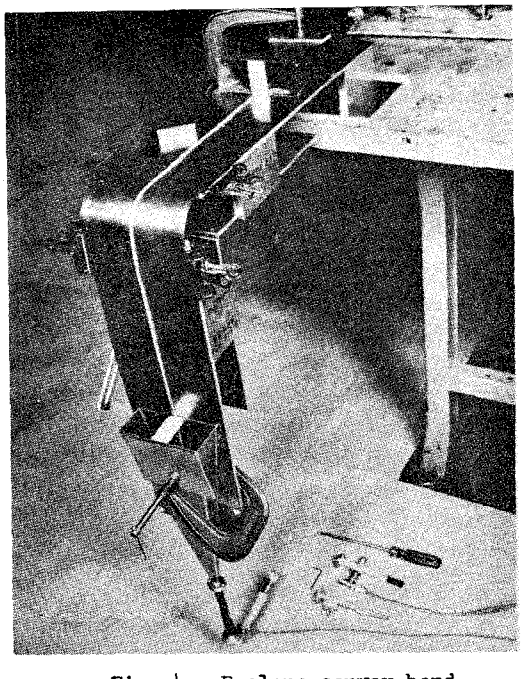

Fig. 4 - E-plane convex bend.

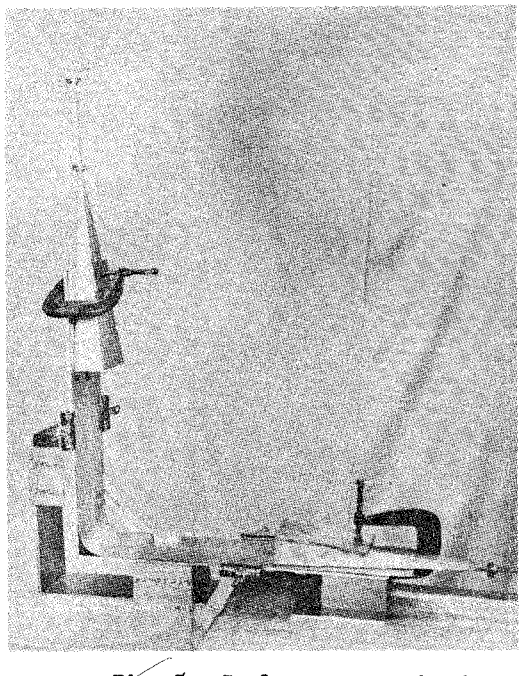

Fig. 5 - E-plane concave bend.

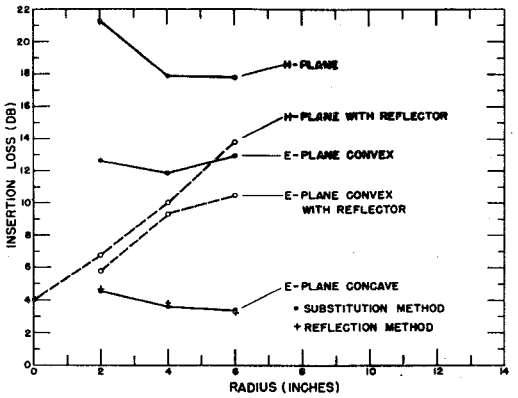

Fig. 6 - Insertion loss of bends in image guide.

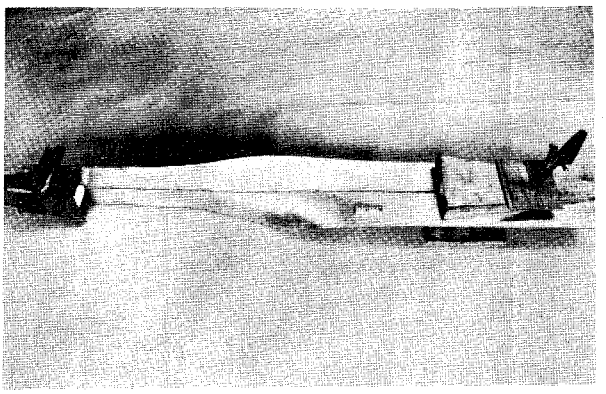

Fig. 7 - Twist section.

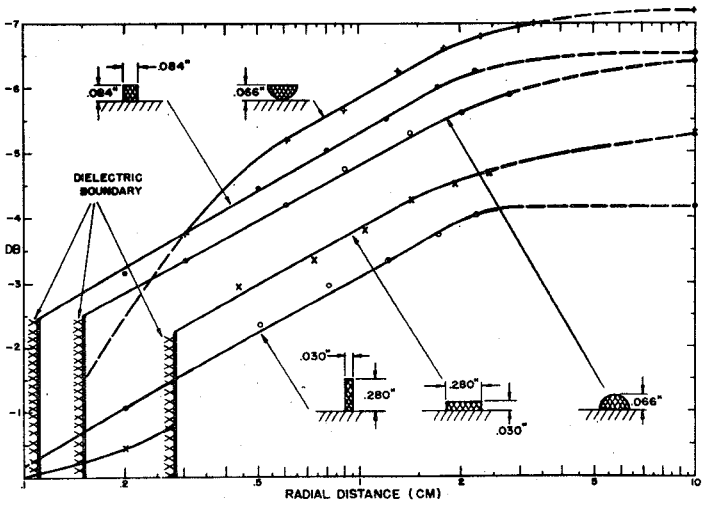

Fig. 8 - Cross-sectional field distributions. The maximum field occurs in the dielectric and is taken as the reference level.

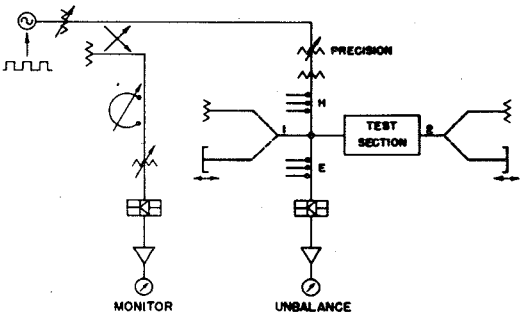

Fig. 9 - System for measuring insertion loss and input reflections.

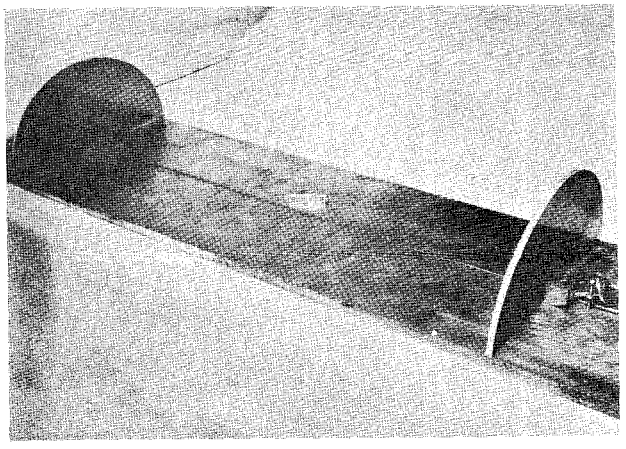

Fig. 10 - Image rod resonator.

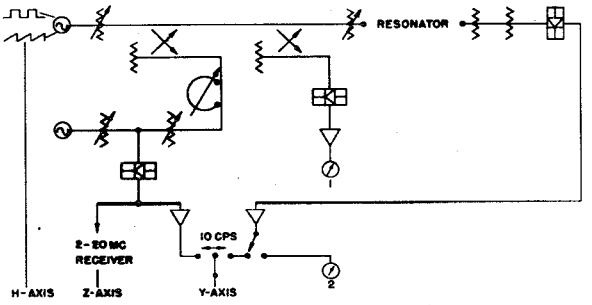

Fig. 11 - System for measuring resonant insertion loss and Q.

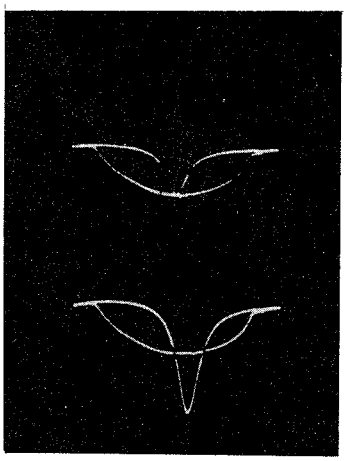

Fig. 12 - Resonance curve displays, with and without 3db attenuation.

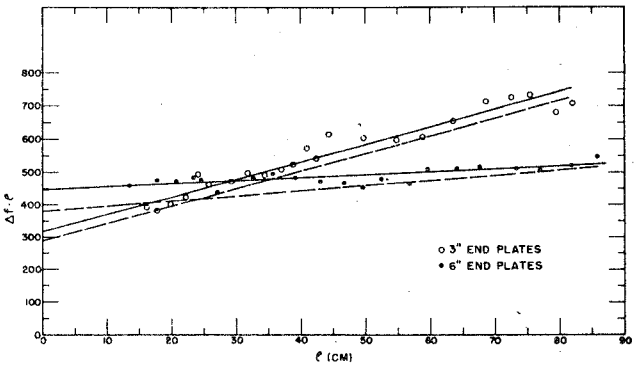

Fig. 13 - Plot of Δf. $\rho \sim \rho/Q$ vs ρ for half-round cross-section.

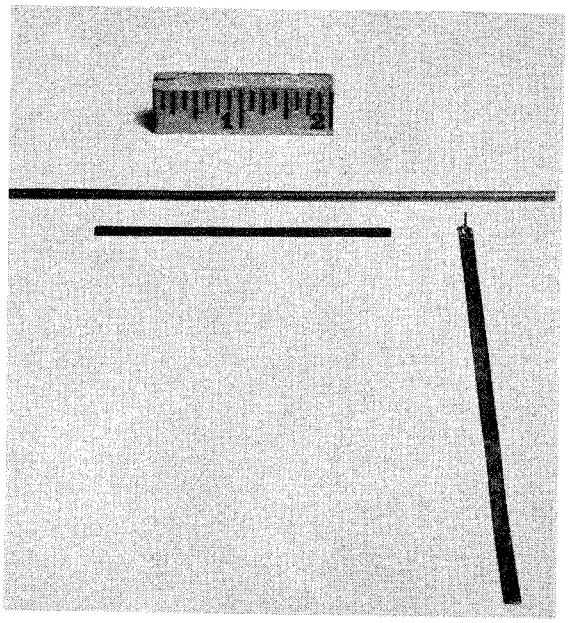

Fig. 14 - Dissipative strip and scatterer.